

Science Advances

- [Facebook](#)
- [Twitter](#)
- [Google+](#)
- [Rss](#)

- [Authors](#)
- [Members](#)
- [Librarians](#)
- [Advertisers](#)

- [Home](#)
- [News](#)
- [Careers](#)



- [Science](#)
- [Science Translational Medicine](#)
- [Science Signaling](#)
-

Science Advances 

- [News](#)

- [Journals](#)

-
-
-
-

- [Careers](#)

Search for this keyword

RESEARCH ARTICLE

Gene therapy rescues disease phenotype in a spinal muscular atrophy with respiratory distress type 1 (SMARD1) mouse model

Monica Nizzardo, Chiara Simone, Federica Rizzo, Sabrina Salani, Sara Dametti, Paola Rinchetti, Roberto Del Bo, Kevin Foust, Brian K. Kaspar, Nereo Bresolin, Giacomo P. Comi, Stefania Corti

[+ Author Affiliations](#)

Science Advances 13 Mar 2015:

Vol. 1 no. 2 e1500078

DOI: 10.1126/sciadv.1500078

- [Article](#)
- [Figures & Data](#)
- [Info & Metrics](#)
- [eLetters](#)
- [PDF](#)

SHARE

- 354
- 6

Abstract

Spinal muscular atrophy with respiratory distress type 1 (SMARD1) is an autosomal recessive motor neuron disease affecting children. It is caused by mutations in the *IGHMBP2* gene (11q13) and presently has no cure. Recently, adeno-associated virus serotype 9 (AAV9)–mediated gene therapy has been shown to rescue the phenotype of animal models of another lower motor neuron disorder, spinal muscular atrophy 5q, and a clinical trial with this strategy is ongoing. We report rescue of the disease phenotype in a SMARD1 mouse model after therapeutic delivery via systemic injection of an AAV9 construct encoding the wild-type *IGHMBP2* to replace the defective gene. AAV9-*IGHMBP2* administration restored protein levels and rescued motor function, neuromuscular physiology, and life span (450% increase), ameliorating pathological features in the central nervous system, muscles, and heart. To test this strategy in a human model, we transferred wild-type *IGHMBP2* into human SMARD1-induced pluripotent stem cell–derived motor neurons; these cells exhibited increased survival and axonal length in long-term culture. Our data support the translational potential of AAV-mediated gene therapies for SMARD1, opening the door for AAV9-mediated therapy in human clinical trials.

INTRODUCTION

Spinal muscular atrophy with respiratory distress type 1 (SMARD1, OMIM 604320), also called distal spinal muscular atrophy type 1, is a fatal genetic motor neuron disease with infantile onset and without any effective therapy ([1](#), [2](#)). It is the second most frequent form of spinal muscular atrophy after spinal muscular atrophy linked to chromosome 5q (SMA). SMARD1 is characterized by respiratory distress, usually within the first year of life, with initially distal and later generalized muscle weakness that leads to early death ([2](#), [3](#)). The disease results from loss-of-function mutations in the gene encoding the immunoglobulin μ -binding protein 2 (*IGHMBP2*) ([4](#), [5](#)). *IGHMBP2* is an adenosine triphosphatase/helicase motif-containing DNA-binding protein that controls several nuclear, RNA, and translation processes; its function remains largely unclear. A splice site mutation in murine *Ighmbp2* causes a neuromuscular disorder in the *nmd* mouse similar to the human disease, thus representing an animal model of SMARD1 ([6](#)).

Although how *IGHMBP2* reduction/loss leads to selective motor neuron degeneration and to the disease phenotype in rodents and humans is unknown, gene therapy is a potential curative therapeutic strategy because it provides a functional gene, thereby addressing the cause of the disease. The final objective in the treatment of neurological disorders is to achieve global distribution of the therapeutic agent via minimally invasive delivery. Adeno-associated virus serotype 9 (AAV9), a recently isolated serotype, displays central nervous system (CNS) tropism and crosses the blood-brain barrier after systemic and intrathecal administration ([7](#), [8](#)). Moreover, systemically delivered AAV9 vectors efficiently transduce numerous peripheral tissues, such as the heart and skeletal muscles, which are affected in SMARD1 ([3](#), [9](#)). Recent gene therapies aiming at *SMN1* AAV9–mediated delivery in SMA mice and large animals, conducted with systemic or cerebrospinal fluid injection, seem promising and may provide some of the most efficacious therapeutic possibilities for SMA patients ([10–13](#)). The Food and Drug Administration recently approved a phase 1 clinical trial to evaluate the safety and efficacy of intravenous delivery of AAV9 human SMN in patients with type I SMA, with an age range of 0 to 9 months. This trial ([NCT02122952](https://clinicaltrials.gov/ct2/show/study/NCT02122952), www.clinicaltrial.gov) started enrolling patients in April 2014; three patients have been injected

(14). No gene therapy strategy has yet been attempted for SMARD1, and few other therapeutic approaches have been tested. We previously performed the first experimental investigations using cell therapy in *nmd* mice (15–17).

Here, we provide preclinical proof-of-principle data that demonstrate the high efficacy of *IGHMBP2* gene therapy in the SMARD1 mouse model as well as in an in vitro model of the human disease, providing strong evidence for establishing a clinical trial of AAV9-mediated *IGHMBP2* gene therapy. In the *nmd* mice investigated here, AAV9-*IGHMBP2* gene transfer via systemic injection resulted in unprecedented improvements in motor function and survival. Wild-type *IGHMBP2* rescued the disease phenotype in human SMARD1 motor neurons in vitro. Furthermore, we established an AAV9-*IGHMBP2* construct and a preclinical administration protocol to serve as a template for future clinical trials for SMARD1 and other genetic diseases of motor neurons.

RESULTS

AAV9-*IGHMBP2* can increase protein levels in wild-type mice

We generated a plasmid harboring a single-stranded AAV expression cassette carrying the wild-type human *IGHMBP2* complementary DNA (cDNA) [National Center for Biotechnology Information (NCBI) accession number [NM_002180](#)] coding sequence under the control of the cytomegalovirus (CMV) enhancer/chicken β -actin (CBA) promoter (fig. S1A) (AAV9-*IGHMBP2*). We transfected human embryonic kidney (HEK) 293 cells with the plasmid, which resulted in up-regulated expression of *IGHMBP2* protein (fig. S1, B and C). Next, we evaluated its potency in C57BL/6 mice by delivering 1×10^{10} vector genomes (vg) of AAV9-*IGHMBP2* to the gastrocnemius muscle via intramuscular injection. Two weeks after injection, *IGHMBP2* levels were clearly detectable in the injected muscle by Western blotting (fig. S1, D and E).

Administration of AAV9-*IGHMBP2* results in high levels of expression in the *nmd* CNS

To define the transduction efficiency of AAV9, we injected *nmd* and wild-type pups at postnatal day 1 (P1) with AAV9 encoding green fluorescent protein (GFP) (AAV9-*GFP*), AAV9-*IGHMBP2*, or AAV9 with no inserted gene (AAV9-null) intravenously into the facial vein for a total dose of 5×10^{11} vg per pup ([Fig. 1A](#)). AAV9-*GFP* injection resulted in widespread central nervous system (CNS) transduction, particularly in the spinal cord, as indicated by the fluorescence intensity of GFP in the parenchyma ([Fig. 1B](#)). SMI32-positive motor neurons were highly positive for GFP after AAV9-*GFP* injection ([Fig. 1C](#)). We observed that 40% of lumbar spinal motor neurons expressed GFP 2 weeks after injection. Thus, intravenous injection in P1 mice led to the broad and extensive transduction of the spinal cord by the genetic construct.

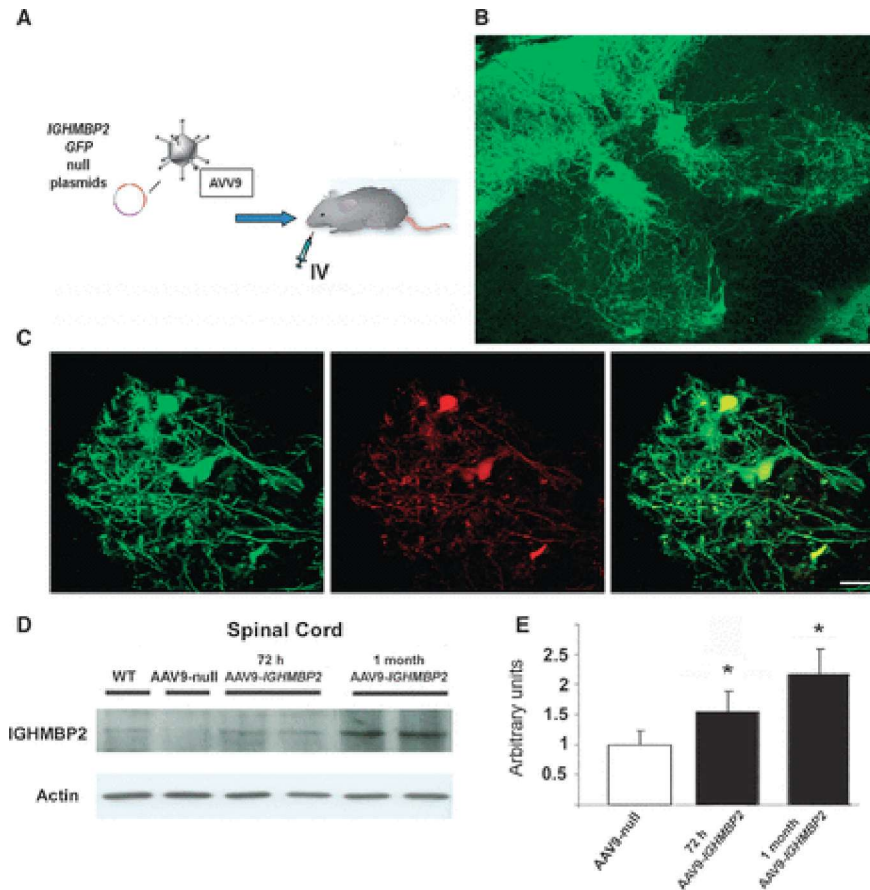


Fig. 1 AAV9-GFP and AAV9-IGHMBP2 efficiently transduce tissues in *nmd* mice.

(A) In vivo experimental design: newborn (P1) *nmd* mice were injected with AAV9-GFP, AAV9-IGHMBP2, or AAV9-null for a total dose of 5×10^{11} vg. (B) Injection of AAV9-GFP in wild-type (WT) animals resulted in GFP expression (green) within the spinal cord 2 weeks after injection. (C) Colocalization of GFP (green) with SMI32 (red) demonstrated that motor neurons were efficiently transduced. (D) Western blots of spinal cords revealed increased levels of IGHMBP2 in AAV9-IGHMBP2-*nmd* versus AAV9-null-*nmd* animals. (E) Quantification of IGHMBP2 levels in the spinal cord. Values are means \pm SEM of IGHMBP2: β -actin expression levels ($n = 5$), $*P < 0.01$. Scale bars, 500 μ m (B) and 50 μ m (C).

- [Download figure](#)
- [Open in new tab](#)

- [Download powerpoint](#)

To measure the increase in IGHMBP2 expression after AAV9 administration, we treated a cohort of wild -type and *nmd* mice at P1 with a single intravenous injection of AAV9 -*IGHMBP2* or AAV9 -null (5×10^{11} vg per pup). AAV9 -*IGHMBP2* treatment resulted in a twofold increase in IGHMBP2 protein levels in spinal cord compared with AAV9 -null treatment ($P < 0.01$; [Fig. 1](#), D and E).

AAV9-*IGHMBP2* therapy protects SMARD1 motor neurons and axons

To evaluate the impact of gene therapy on neuropathological SMARD1 hallmarks, we analyzed spinal cord motor neurons and ventral spinal nerve roots in 4-week-old mice. We detected a severe loss of motor neurons in AAV9 -null-*nmd* mice compared to wild-type mice ([Fig. 2](#)). In contrast, in association with the increase in IGHMBP2 expression, we detected consistent preservation of the number of motor neurons in AAV9 -*IGHMBP2*-*nmd* mice ([Fig. 2A](#)). In all analyzed sections, the number of motor neurons in AAV9 -*IGHMBP2*-*nmd* mice was significantly higher than that in AAV9 -null-*nmd* littermates ($P < 0.01$; [Fig. 2B](#)).

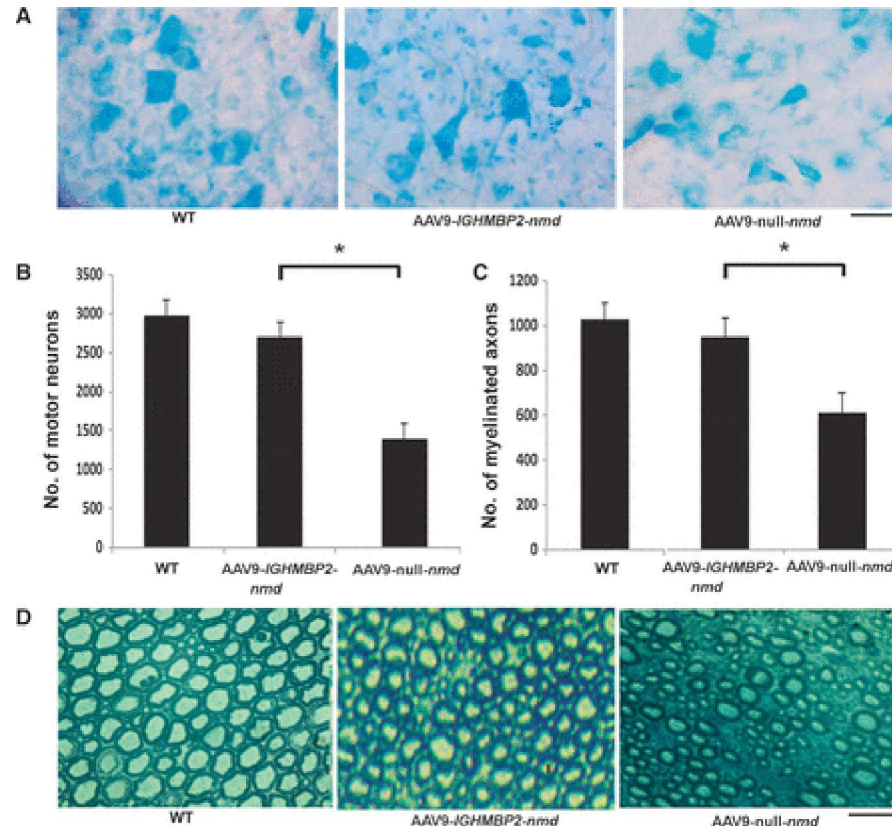


Fig. 2 AAV9-IGHMBP2 increases motor neuron and axon number.

(A) Representative motor neuron pools in the lumbar segment of the spinal cords of AAV9-IGHMBP2-nmd, AAV9-null-nmd, and WT mice at 4 weeks of age. (B) Quantification of motor neurons in the lumbar spinal cords of treated mice and WT mice (mean ± SD) at 4 weeks of age ($n = 6$ per group per time point). (C) Quantification of myelinated axons in the L4 anterior roots in WT, AAV9-IGHMBP2-nmd, and AAV9-null nmd mice (mean ± SD) at 4 weeks of age ($n = 6$ per group per time point). Motor neuron and myelinated axon counts significantly increased in the AAV9-IGHMBP2 treatment group compared to the AAV9-null group ($*P < 0.0001$). (D) Representative images of the L4 anterior roots of AAV9-IGHMBP2-nmd, AAV9-null-nmd, and WT mice at 4 weeks of age. Scale bar, 50 μm (A and D).

- [Download figure](#)
- [Open in new tab](#)
- [Download powerpoint](#)

Prominent motor neuron degeneration significantly reduced the number and overall diameter of L4-L5 ventral nerve roots in AAV9 -null-*nmd* mice ([Fig. 2D](#)). The same reduction was detected in all lumbar ventral roots analyzed ([Fig. 2D](#)). Significant improvement occurred after treatment; 4-week-old AAV9 -null-*nmd* mice displayed fewer myelinated axons, whereas the number of myelinated axons in the ventral roots of AAV9 -*IGHMBP2-nmd* mice was significantly restored ($P < 0.01$; [Fig. 2C](#)).

Wild-type gene delivery ameliorates defects in neuromuscular junctions

Mutant *nmd* mice had denervated motor end plates that correspond to motor neuron degeneration ([Fig. 3](#), A and B). In these motor endplates, subsynaptic clefts and folds were not present and/or did not mature, indicating degeneration ([Fig. 3A](#)). We observed this pathological hallmark of SMARD1 disease in nearly 50% of presynaptic termini from the quadriceps, gastrocnemius, and diaphragm of AAV9 -null-*nmd* animals ([Fig. 3B](#)). On the other hand, nearly 90% of neuromuscular junctions (NMJs) of the AAV9 -*IGHMBP2-nmd* mice were innervated and did not present this abnormal structure ([Fig. 3](#), A and B). We observed a correct “pretzel-like” structure on postsynaptic NMJs that reflected the presence of a functional network of acetylcholine receptors in AAV9 -*IGHMBP2-nmd* mice ([Fig. 3A](#)).

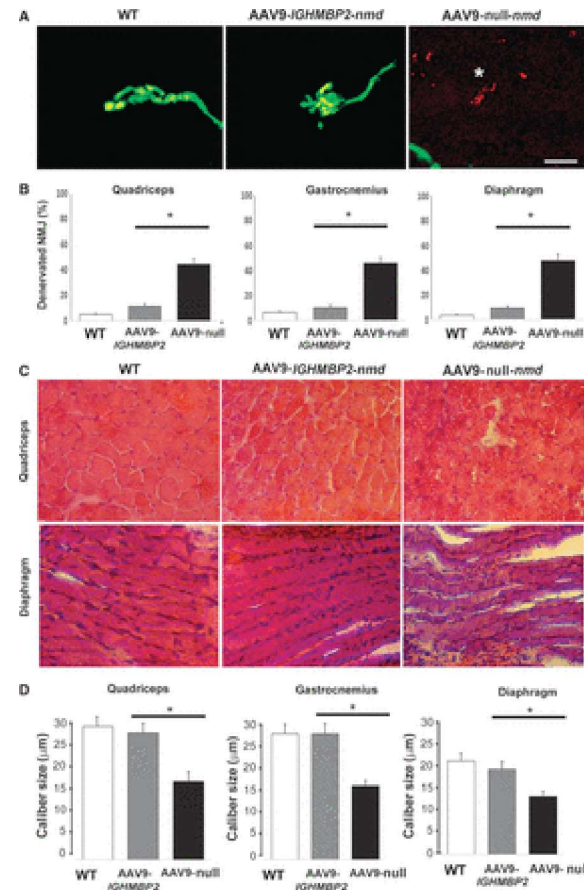


Fig. 3 AAV9-IGHMBP2 improves NMJs and the size of myofibers in skeletal muscles.

(A and B) NMJs in the quadriceps, gastrocnemius, and diaphragm muscles improved after gene therapy. (A) Representative images of NMJs from the quadriceps of WT, AAV9-IGHMBP2-nmd, and AAV9-null-nmd mice. Neurofilament Ab, green; α -bungarotoxin, red. The asterisk highlights an unoccupied NMJ. Scale bar, 20 μ m. (B) Percentage of denervated NMJs in gastrocnemius, quadriceps, and diaphragm muscles (mean \pm SEM; * $P < 0.001$). (C and D) AAV9-IGHMBP2 treatment influenced fiber caliber in nmd quadriceps, gastrocnemius, and diaphragm muscles. (C) Representative images of quadriceps and diaphragm muscle fibers at 4 weeks stained with hematoxylin and eosin (H&E). Increased numbers of perimysial and central cell nuclei were observed in untreated nmd mice; these numbers declined after AAV9-IGHMBP2 treatment. Scale bar, 100 μ m. (D) Significant reductions in fiber caliber were evident in AAV9-null-nmd mice versus control mice; AAV9-IGHMBP2 treatment ameliorated this effect. Values are means \pm SEM.

- [Download figure](#)
- [Open in new tab](#)
- [Download powerpoint](#)

AAV9-IGHMBP2 improves the size of myofibers in skeletal muscles and heart

Nmd mice typically display muscle fiber atrophy in gastrocnemius and diaphragm muscles, mimicking the human pathological condition in SMARD1 (2, 18). These aspects are due to denervation and to myopathic changes caused by IGHMBP2 reduction. We confirmed severe myopathic changes, including a wide variability in fiber size, centralized nuclei, fatty infiltration, and necrotic myofibers, in the quadriceps and diaphragm of AAV-null-*nmd* mice (Fig. 3C).

In contrast, AAV9-IGHMBP2 treatment positively affected muscle fiber morphology and organization and significantly increased myofiber caliber in the quadriceps, gastrocnemius, and diaphragm ($P < 0.001$; Fig. 3, C and D). Because a previous study uncovered signs of cardiomyopathy in *nmd* mice (19), we performed pathological analysis and weight measurement of the heart. AAV-null-*nmd* mice had mild cardiac hypertrophy that was slightly improved, even if not statistically significant, with AAV-IGHMBP2 treatment, as measured by the ratio of heart weight to body weight (fig. S2).

AAV9-IGHMBP2 therapy rescues the neuromuscular phenotype and increases the survival of SMARD1 mice

We evaluated whether AAV9-IGHMBP2 treatment improved the disease phenotype and extended survival in *nmd* mice. Functional recovery was assessed in all animal groups through blind evaluation of their general appearance, weight, neuromuscular function, and survival after treatment (Fig. 4). The first clinical symptoms in *nmd* mice presented in the second postnatal week when mice rapidly developed muscle weakness in the hindlimbs, which were contracted, causing impaired locomotor activity. This limited limb extension made standing on all four limbs impossible. Suspended by the tail, homozygous affected mice were not able to clench their hindlimbs and could not grip a cage cover (Fig. 4A). As the disease progressed, this weakness worsened to include the forelimbs and trunk muscles, as previously reported (18–20).

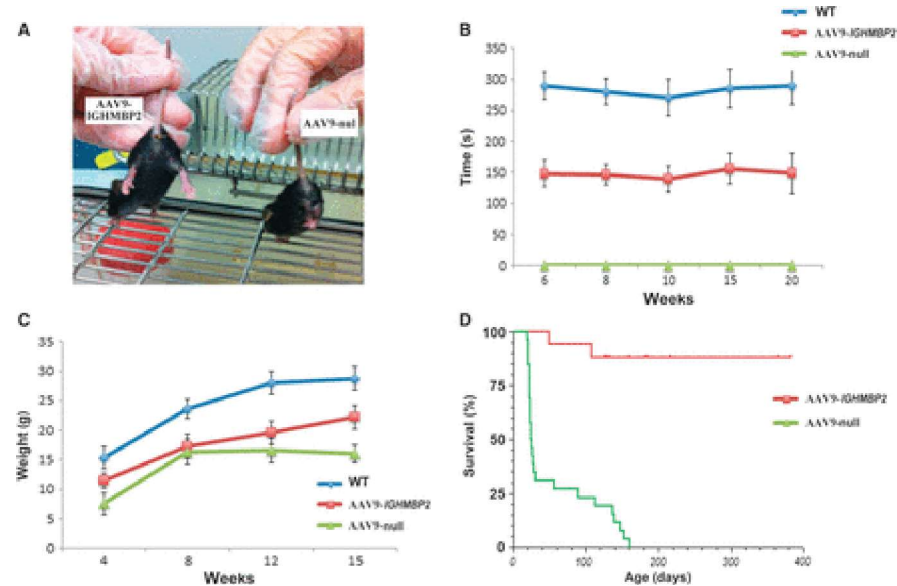


Fig. 4 AAV9-IGHMBP2 treatment improves neuromuscular function and survival in *nmd* mice.

(A) Representative images of AAV9-IGHMBP2-*nmd* mice showing their capacity to extend their hindlimbs in comparison to AAV9-null-*nmd* mice. (B) Rotarod test data. The performance of AAV9-IGHMBP2-*nmd* mice was significantly improved versus AAV9-null-*nmd* mice, which were never able to complete the test ($P < 0.0001$). Error bars denote SEM. (C) The mean body weight of AAV9-IGHMBP2-*nmd* mice significantly increased relative to AAV9-null-*nmd* mice ($P < 0.01$). Error bars show SEM. (D) Kaplan-Meier survival curves of AAV9-IGHMBP2-*nmd* mice and AAV9-null-*nmd* mice ($P < 0.0001$). For all graphs: AAV9-IGHMBP2-*nmd* mice, $n = 17$; AAV9-null-*nmd* mice, $n = 24$.

- [Download figure](#)
- [Open in new tab](#)
- [Download powerpoint](#)

Gross examination of AAV9-IGHMBP2-*nmd* animals revealed an improved appearance relative to AAV9-null-*nmd* mice; treated animals were more similar to wild-type animals (movie S1). Most AAV9-IGHMBP2-*nmd* mice exhibited no overt signs of motor dysfunction and were nearly indistinguishable from their wild-type littermates (movie S1); they were able to walk, explore the environment, and perform various behaviors like wild-type mice. At 3 weeks, AAV9-IGHMBP2-*nmd* mice could splay their hindlimbs (Fig. 4A). In contrast, their AAV9-null-*nmd* littermates showed muscle degeneration and clear contracture of the hindlimbs (Fig. 4A).

AAV9-null-*nmd* mice were paralyzed by the age of 5 weeks and failed to remain on the accelerating rotarod test for more than a few seconds ($P < 0.0001$ versus wild-type siblings) (**Fig. 4B**), as previously described (**19**). In contrast, AAV9-*IGHMBP2-nmd* mice could perform the rotarod test throughout their lifetimes and did not display a hindlimb clasp. At each time point, the performance of AAV9-*IGHMBP2-nmd* mice was superior to that of AAV9-null-*nmd* animals ($P < 0.0001$ versus AAV9-null-*nmd* mice; **Fig. 4B**). The growth rate of AAV9-*IGHMBP2-nmd* mice, as measured by mean body weight, increased compared to that of AAV9-null-*nmd* mice and was significantly different (weeks 4, 12, and 15, $P < 0.01$; week 8, $P < 0.05$; **Fig. 4C**). More strikingly, Kaplan-Meier survival estimates revealed that AAV9-*IGHMBP2-nmd* mice showed significantly increased mean life spans (450%) compared to sibling-matched AAV9-null-*nmd* mice (AAV9-*IGHMBP2-nmd*, 307 ± 74 days, $n = 17$; AAV9-null-*nmd*, 68 ± 25 days, $n = 24$; $P = 0.0001$, $\chi^2 = 26.52$; **Fig. 4D**). Most AAV9-*IGHMBP2-nmd* animals are still alive, some at more than 300 days of age, suggesting that they can be considered completely rescued.

AAV9-*IGHMBP2* rescues the disease phenotype of spinal motor neurons derived from SMARD1-induced pluripotent stem cells (iPSCs)

Our next question was whether the transfer of *IGHMBP2* also protected human SMARD1 motor neurons against degeneration induced by the loss of *IGHMBP2*. For this purpose, we used iPSCs that we generated from SMARD1 patients and healthy subjects (**Fig. 5A**) (**17**). We differentiated these cells into motor neurons, monitoring their phenotype by immunocytochemistry for motor neuronal markers. Human motor neurons extended processes and expressed SMI32 and choline acetyltransferase (ChAT) (**Fig. 5B**). For further evaluation, we examined several features of motor neurons that are likely relevant to SMARD1 pathogenesis, including cell survival, axonal elongation, and growth cone formation. At 8 weeks, SMARD1 iPSC-derived motor neurons had significantly reduced cell numbers and axon length compared to motor neurons derived from wild-type iPSCs ($P < 0.001$). However, motor neurons derived from genetically corrected SMARD1 cells (TR-SMARD1) presented an ameliorated phenotype, with increased cell survival at 8 weeks of culture ($P < 0.001$; **Fig. 5C**). These improved features were linked to increased *IGHMBP2* expression; TR-SMARD1 motor neurons also presented increased neurite lengths compared to untreated neurons ($P < 0.001$; **Fig. 5D**). TR-SMARD1 motor neurons and their parental iPSCs expressed *IGHMBP2* at higher levels than did untreated cells, as revealed by immunocytochemistry and Western blotting (**Fig. 5**, E to G). Thus, transferring wild-type *IGHMBP2* can protect human motor neurons from SMARD1-induced degeneration.

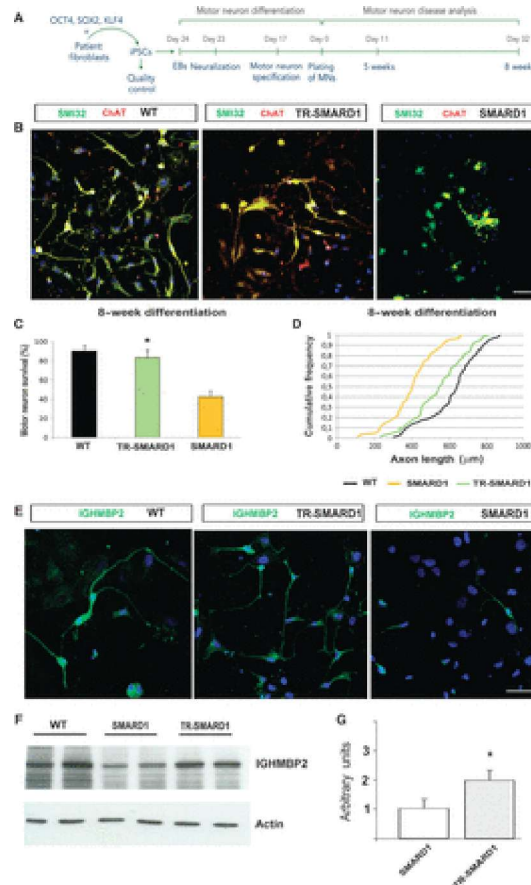


Fig. 5 AAV9-IGHMBP2 treatment protects human iPSC-derived spinal motor neurons from SMARD1-induced degeneration.

(A) Schematic of the experimental strategy used to differentiate motor neurons from iPSCs. (B) Compared to WT (left), significantly fewer SMARD1 motor neurons were observed after long-term culture (right). Genetic correction with *IGHMBP2* increased the number of SMARD1 motor neurons (TR-SMARD1, middle panel). SMI32, green; ChAT, red; DAPI, blue. Scale bar, 75 μ m. (C) Genetic correction (green bar) protected motor neurons in long-term culture, increasing their survival versus SMARD1 cells (yellow bar) (8 weeks, * $P < 0.001$). (D) At 8 weeks, SMARD1 motor neurons (yellow) presented shorter axons than did WT cells (black). TR-SMARD1 (green) had longer axons than did SMARD1 motor neurons ($P < 0.001$). (E) IGHMBP2 staining (green) of WT motor neurons (left), SMARD1 motor neurons (right), and TR-SMARD1 (middle). Nuclei were counterstained with DAPI (blue). Scale bar, 70 μ m. (F) Western blot of genetically corrected SMARD1 iPSCs (TR-

SMARD1) indicated significantly increased expression of IGHMBP2 with respect to SMARD1 cells (SMARD1). (G) Quantification of IGHMBP2 levels in transfected SMARD1 iPSCs (TR-SMARD1) versus untransfected SMARD1 cells (SMARD1). Values are means \pm SEM (* $P < 0.01$).

- [Download figure](#)
- [Open in new tab](#)
- [Download powerpoint](#)

DISCUSSION

SMARD1 is a motor neuron disease caused by mutations in *IGHMBP2*. Because it is due to a single gene defect and has a fatal outcome without any effective cure, it could be an appropriate candidate disease for therapeutic strategies based on gene therapy.

Here, we demonstrated the efficacy of AAV9-mediated induction of wild-type *IGHMBP2* expression, a strategy that may represent a novel and successful therapeutic approach for SMARD1. We described the most effective rescue of SMARD1 mice achieved with a therapeutic treatment to date; this rescue was characterized according to motor function, neuromuscular physiology, and survival after a single injection of AAV9-*IGHMBP2*. We systemically administered AAV9 vectors encoding human wild-type *IGHMBP2*, exploiting the cutting edge finding that AAV9 can cross the blood-brain barrier and successfully transduce the CNS (7, 8). These results were obtained in the *nmd* mouse model, which recapitulates many disease features of SMARD1 patients (1). Our study verified that the reconstitution of IGHMBP2 levels in the CNS and in systemic organs corrected the pathological manifestations in these organs. More strikingly, we achieved the longest extensions in survival ever reported for the *nmd* mouse model (increasing survival by 450%); the phenotype of some AAV9-*IGHMBP2-nmd* animals was nearly indistinguishable from that of their wild-type littermates.

Previous investigations indicated that IGHMBP2 expression, not only in motor neurons but also in other types of cells, is required to obtain complete functional rescue of the *nmd* phenotype (18, 19). Indeed, neuron-specific expression of IGHMBP2 rescued motor neuron degeneration in *nmd* mice, but not the cardiac and skeletal myopathies that lead to the death of *nmd* mice (19). These data suggest an additional role of IGHMBP2 in the conservation of muscle fibers. Systemic injection allowed us to treat not only neurons and nonneuronal cells but also muscle and heart, all of which are involved in SMARD1 pathogenesis and are target cells for SMARD1 treatment.

AAV9-*IGHMBP2* treatment consistently preserved the numbers of motor neurons and axons in SMARD1 mice, even if we achieved 40% transduction of motor neurons. We hypothesize that the overall increase in IGHMBP2 levels in various cell compartments—not only the soma but also at the NMJ site and in other cells, such as nonneuronal cells in the CNS and muscles in the periphery—contributes to the observed increases in motor neuron survival. Indeed, *IGHMBP2* delivery repaired the abnormal architecture of pre- and postsynaptic NMJs, which is also associated with functional improvements on the rotarod test. Myofiber size and NMJ structure in AAV9-*IGHMBP2-nmd* mice were similar to those in wild-type

muscles. This result may be due to the direct action of IGHMBP2 on NMJs, favoring the normalization of transcription/translation in presynaptic termini, as well as to direct IGHMBP2 action on muscle. AAV9-IGHMBP2 treatment also exerted a positive effect on muscle fiber morphology and organization and significantly increased myofiber caliber in the quadriceps, gastrocnemius, and diaphragm. Correcting defects in the CNS, heart, and muscles likely facilitated the long-term survival in this animal model. Treating dilated cardiomyopathy is an important aspect of rescuing these animal models, an aspect that can be overlooked in humans because of the severity of CNS clinical features. The myopathy observed in *nmd* mice has not been clearly detected in human SMARD1 patients, probably because severe motor neuropathy causes death before cardiomyopathy manifestation (19). Further studies are needed to understand whether targeting other tissues and organs in addition to the CNS is necessary in humans.

For clinical translation, the widespread transfer of the gene to the brain and the spinal cord resulting from a peripheral injection is particularly important because it allows a minimally invasive intervention, avoids direct injecting directly the CNS, and produces gene expression throughout the entire CNS. Moreover, the probability of an immunoresponse against IGHMBP2 in children is relatively low, because many SMARD1 patients have a residual amount of protein. Quantification of this residual amount of protein is possible before treatment, for example, in peripheral cells such as fibroblasts (21), thus allowing the evaluation of immunization risk if the protein is absent. Immunosuppression with steroids can mitigate the immune response, as demonstrated with gene therapy for Duchenne muscular dystrophy (22). Although the AAV capsid can raise an immunoresponse, one-time gene therapy may be suitable for the reasons discussed above; some strategies, such as plasmapheresis, can eliminate the negative impact of antibodies (Abs) against AAV (23).

Another advantage of AAV9-mediated gene delivery is that it leads to long-term wild-type protein expression after a single injection. For clinical trials, this construct can be administered both into the bloodstream and locally into the cerebrospinal fluid.

This study demonstrated that gene therapy is highly efficacious when applied at birth in presymptomatic *nmd* mice, defining a window of opportunity for treating SMARD1. However, SMARD1 children are often asymptomatic at birth, and even if newborn screening is feasible, it is crucial to investigate whether treatment is also efficacious when administered during a symptomatic phase. In the future, we plan to conduct further experiments to define the effective therapeutic window. At first glance, there may be a possible narrow window of opportunity for therapeutic intervention in SMARD1 on the basis of findings from SMA. In a current gene therapy-based clinical trial for SMA, patients are treated at diagnosis (when the first symptoms appear, www.clinicaltrials.gov, [NCT02122952](https://clinicaltrials.gov/ct2/show/study/NCT02122952)). Even for rare diseases such as SMARD1, newborn screening can become feasible when a treatment approach becomes effective. Recently, a combination of exome and Sanger sequencing linked mutations affecting *IGHMBP2* to a milder phenotype similar to CMT2 (21); in these patients, no respiratory compromise occurs. In that study, although IGHMBP2 protein levels were lower than those in control subjects, they were significantly higher in cells from patients affected by CMT2 than in cells from SMARD1 patients, suggesting that differences in clinical phenotype are related to IGHMBP2 protein levels. These data broaden the number and spectrum of patients that can be treated with our approach. No effective treatments are available for SMARD1; gene therapy is a promising strategy, not only because it can reverse the disease but also because it can prevent further deterioration.

Gene therapy approaches for SMA and SMARD1 are similar. The diseases are both autosomal recessive disorders that affect mainly children through loss-of-function mutations in a protein whose levels are reduced, leading to the degeneration of motor neurons. Age of onset and progressive paralysis are similar for the two disorders. Nevertheless, some differences must be considered. First, the *IGHMBP2* transgene is larger than the *SMN* gene and can only be accommodated in linear (not self-complementary) AAV9. However, we did not observe a significant reduction in construct delivery or cell transfection efficacy, and good rescue of the animals was achieved.

We further evaluated the effect of gene therapy in the context of human disease, using human SMARD1 iPSC-derived motor neurons as in vitro model. We observed rescue of the SMARD1 phenotype after ex vivo genetic correction; improvements in cell survival, axonal elongation, and growth cone formation confirmed that transferring wild-type *IGHMBP2* protects motor neurons from SMARD1-induced degeneration in vitro. Previous studies (17, 18) that analyzed the survival and neurite length of primary motor neurons isolated from SMARD1 mice did not show any difference in survival or axon length compared to wild-type cells under basal conditions; survival was reduced in a neurotoxic environment, which was provided by lipopolysaccharide-activated microglial-conditioned medium. This discrepancy between rodent data and data from human SMARD1 motor neurons, in which reduced survival is evident, is mirrored in the SMA field. SMA murine motor neurons do not show a decrease in survival that is apparent in human SMA iPSC-derived motor neurons (24, 25). The reasons underlying this discrepancy are unknown and are perhaps due to different residual protein levels in combination with model-based differences (species, transgenes, etc.). Our in vitro and in vivo experiments provide an excellent rationale for clinical translation to patients.

In summary, *IGHMBP2* gene therapy resulted in a highly efficacious rescue of survival and of the pathological phenotype of a SMARD1 mouse model. Systemic administration was necessary and sufficient to target both neuronal and muscular pathological features. This study confirms the feasibility of AAV-based technologies as effective therapeutic strategies for the treatment of genetic motor neuron diseases. In particular, our results provide a proof of principle for the feasibility of clinical translation of this strategy to treat SMARD1 and other genetic motor neuron disorders.

MATERIALS AND METHODS

AAV vectors

The open reading frame of the human *IGHMBP2* cDNA (NCBI accession number [NM_002080](#)) was cloned into a shuttle plasmid containing either AAV2 inverted terminal repeats (ITR) and the 1.6-kb CBA promoter. Single-stranded AAV9-IGHMBP was produced by transient transfection of HEK293 cells using a double-stranded AAV2-ITR-based CBA vector with a plasmid encoding Rep2Cap9, as previously described (7), along with an adenoviral helper plasmid (pHelper, Stratagene). Our serotype 9 sequence was verified by sequencing; it was identical to the sequence previously described (7). Virus was purified by two cesium chloride density gradient purification steps, dialyzed against phosphate-buffered saline (PBS), formulated with 0.001% Pluronic F-68 to prevent virus aggregation, and stored at 4°C. All vector preparations were titered through quantitative polymerase chain reaction (PCR), using TaqMan technology (Life Technologies). Vector purity was assessed by 4 to 12% SDS-polyacrylamide gel electrophoresis (SDS-PAGE) and silver staining (Life Technologies). We used a single-stranded AAV9 encoding GFP under control of the CMV

promoter (AAV9-*GFP*) to monitor transduction efficacy. As a control, a third vector was generated in which the IGHMBP2 cDNA was replaced with a noncoding sequence under the CBA promoter to generate AAV9 -null vector.

Animal procedures

The *nmd* mouse (B6.BKS *Ighmbp2nmd-2 J/J*) has a homozygous mutation in *Ighmbp2*. Heterozygous mice were bred to generate mice homozygous for the mutation. Homozygous *nmd* mutant mice and wild-type littermates were used for the experiments and analyses. The genotypes of the mice were confirmed using a PCR-based assay with genomic DNA from tail biopsies, as described previously (6). All transgenic animals were purchased from The Jackson Laboratory. All animal experiments were approved by the University of Milan and Italian Ministry of Health review boards, in compliance with U.S. National Institutes of Health *Guide for the Care and Use of Laboratory Animals* (15).

On P1, pups received one injection in the facial vein; the AAV9-*IGHMBP2/GFP* dose was 5×10^{11} vg in 100 μ l. Systemic injection was performed with a 0.5-ml, 30-gauge insulin syringe (7, 11). As controls, *nmd* mice received AAV9 -null vector using the same dose and surgical procedure. The experimental groups included 17 AAV9-*IGHMBP2-nmd* mice and 24 AAV9 -null-*nmd* mice. A blinded examiner evaluated the animals for weight, rotarod performance, survival record, and histological evaluation. This study was designed so that littermates were distributed equally between the AAV9-*IGHMBP2* and AAV9 -null groups. Additional separate groups of animals (each composed of six mice per time point per condition) were sacrificed for histological analysis, quantification of motor neurons and axons, and muscle analysis. To test AAV9-*IGHMBP2* efficiency, C57BL/6 mice were injected directly in the gastrocnemius with 1×10^{10} vg AAV9-*IGHMBP2*, and muscle was collected after 2 weeks.

Western blots

Western blot analysis for IGHMBP2 was performed as previously described (18, 24). Briefly, frozen spinal cord specimens were homogenized in radioimmunoprecipitation assay buffer [50 mM tris (pH 7.5), 150 mM NaCl, 1% NP-40, 0.5% sodium deoxycholate, and 0.1% SDS] supplemented with protease inhibitor cocktail tablets (Roche). Protein content was measured with the Lowry assay. Cell extracts from HEK293 cells, wild-type iPSCs, and SMARD1 iPSCs were prepared 48 hours after transfection. Forty micrograms of total protein was boiled in Laemmli buffer for 5 min and separated on 8% SDS-PAGE. After electrophoresis, proteins were transferred onto a nitrocellulose membrane, blocked with 5% bovine serum albumin (BSA) for 1 hour at room temperature, and incubated with primary anti-IGHMBP2 peptide antiserum (dilution 1:2500 in 5% BSA, provided by K. Grohmann, Institute for Clinical Neurobiology University of Wuerzburg, Germany) or anti-recombinant IGHMBP2 Ab (1:1500, Sigma-Aldrich) overnight at 4°C. The next day, the nitrocellulose membrane was incubated with anti-rabbit immunoglobulin G conjugated to horseradish peroxidase (1:2700) (18). Finally, immune complexes were detected using chemiluminescence reagents. The nitrocellulose membrane was stripped and reprobed with anti-actin monoclonal Ab (1:1000, Sigma-Aldrich) as a control for equal loading.

Immunohistochemistry and NMJ staining

For histological analysis, 4-week-old animals were sacrificed, perfused, and fixed with 4% paraformaldehyde in PBS (pH 7.4). The spinal cord was isolated, immersed in paraformaldehyde solution for 1 hour followed by incubation in 20% sucrose solution in PBS (pH 7.4) overnight, and frozen in Tissue-Tek optimal cutting temperature compound with liquid nitrogen. The quadriceps, gastrocnemius, and diaphragm muscles of each mouse were used for NMJ analysis.

Muscle fibers from the quadriceps, gastrocnemius, and diaphragm muscles were stained as previously reported (22). Tissues were cryosectioned and mounted on gelatinized glass slides. Every 10th section of 20 μm was collected. All sections were washed with 1 \times PBS, then blocked with 10% BSA in 1 \times PBS and 0.3% Triton X-100 for 1 hour at room temperature. Primary Abs were added overnight at 4°C (neurofilament clone 2H3, 1:100, Developmental Studies Hybridoma Bank; SMI32, 1:200, Millipore; anti-GFP 488, 1:400, Life Technologies). Mouse and rabbit Abs conjugated with Alexa 488 or Alexa 546 (1:400, Life Technologies) or α -bungarotoxin 555 (1:500; Life Technologies) were used for 2 hours at room temperature as secondary Abs when unconjugated primary Abs were used. For NMJ quantification, a minimum of 100 NMJs from each muscle were randomly selected and assessed under a microscope to determine the number of denervated/degenerated NMJs for each muscle group per animal.

Motor neuron and axon counting

The lumbar spinal cord region of 4-week-old animals was processed for paraffin embedding. Serial cross sections (12 μm thick) of the lumbar spinal cords were made, and every fifth section was processed and Nissl-stained with methylene blue, as reported previously (17). The number and diameter (soma) of all motor neurons counted in these cross sections ($n = 50$ for each mouse) were analyzed. The sections were analyzed at $\times 40$ magnification in the anterior horn (either left or right) for the presence of all neurons in that region. All cells were counted within the ventral horn below an arbitrary horizontal line drawn from the central canal. Only neuronal cells with at least one nucleolus located within the nucleus were counted, as previously described (17). The axonal count was performed as previously described on semithin transverse sections stained with toluidine blue (15). Lumbar anterior roots were examined for axon counting on an optic microscope at $\times 60$ magnification.

Morphological analysis of muscles and heart

For histological analysis of the periphery, the nitrogen-frozen quadriceps, gastrocnemius, and diaphragm muscles from each 4-week-old mouse were cryosectioned and stained with H&E to determine myofiber dimensions, as previously reported (24). About 500 nonoverlapping myofibers from each muscle were randomly selected and photographed at $\times 40$ magnification. The cross-sectional area of each myofiber was measured using Metamorph (Molecular Devices) to calculate the overall average myofiber size per muscle for each animal. The weights of hearts from AAV9 - *IGHMBP2-nmd*, AAV9 -null-*nmd*, and wild-type mice were assessed in relation to body weight.

Neuromuscular evaluation and survival

All groups of *nmd* mice were monitored daily after injection of the construct or vehicle for phenotypic hallmarks of disease. The investigators that executed the functional assessment were blinded to treatment status. Body weight was recorded, and motor function was tested weekly with an accelerating rotarod device (4 to 40 rpm, Rota-Rod 7650, Ugo Basile). We recorded the length of time that each mouse remained on the rotarod. Mortality was scored as age at death. The animals were sacrificed when they were unable to right themselves within 30 s of being placed in a supine position (17); examiners were blinded to treatment status.

iPSCs, genetic correction, and differentiation into motor neurons

iPSC lines were reprogrammed from SMARD1 fibroblasts and healthy subjects (from EuroBioBank with appropriate ethical approval) using a nonviral protocol (17). For genetic correction of the SMARD1 iPSC line and the HEK293 line, 1×10^6 cells were transfected with 5 μ g of IGHMBP2 plasmid as previously described (26). To differentiate spinal motor neurons, we followed a multistep protocol developed for human embryonic stem cells and iPSCs (25), using SMARD1 and wild-type iPSCs. Cells were plated with neuronal medium [Dulbecco's modified Eagle's medium/F12 (Life Technologies)] supplemented with MEM Non-Essential Amino Acids Solution (Life Technologies), N2 (Life Technologies), and heparin (2 mg/ml; Sigma-Aldrich), to which retinoic acid (0.1 μ M; Sigma-Aldrich) was added after 10 days for neural caudalization. Posteriorized neuroectodermal cells were collected at day 17 and suspended for 1 week in the same medium with retinoic acid (0.1 μ M) and sonic hedgehog (100 to 200 ng/ml; R&D Systems), followed by the addition of brain-derived neurotrophic factor and glial cell line–derived neurotrophic factor on day 24 (10 ng/ml; PeproTech). A centrifugation gradient was used to maximize motor neuron acquisition (25). Cells were fixed and immunostained for quantification after culture for at least 24 hours.

Immunocytochemistry of iPSC-derived motor neurons

Cells were fixed in 4% paraformaldehyde for 10 min, permeabilized with 0.25% Triton X-100, and blocked with 10% BSA in $1 \times$ PBS and 0.3% Triton X-100 for 1 hour at room temperature. We incubated the cells with primary Abs against IGHMBP2 (1:100, Sigma-Aldrich), SMI-32 (1:100, Covance), or ChAT (goat polyclonal, 1:250, Millipore) overnight and with fluorescein isothiocyanate–conjugated anti-rabbit or anti-mouse (1:100, Dako) or Alexa Fluor 594–conjugated anti-goat (1:400, Life Technologies) secondary Ab for 1.5 hours at room temperature.

For all imaging, we used a confocal Leica LCS2 microscope. We quantified motor neurons by identifying cells positive for motor neuron markers in 10 randomly selected fields per well (three wells per condition per experiment in five experiments). Morphometric axonal length was measured using soma diameter and the distance between two points.

Statistical analysis

Kaplan-Meier survival analysis and log-rank test were used for survival comparisons. Growth curve and strength assay results were analyzed by analysis of variance (ANOVA) followed by Bonferroni's post hoc analysis for multiple comparisons. The number and size of motor neurons, axon

data, myofiber area, and heart measures were evaluated with one-way ANOVA followed by Bonferroni's post hoc analysis. We used StatsDirect for Windows (version 2.6.4) for all analyses, and the null hypothesis was rejected at the 0.05 level. We analyzed differences in the results of morphometric axonal length measurement (mean \pm SEM for five independent experiments) with the Kolmogorov-Smirnov test (www.physics.csbsju.edu/stats/KS-test.n.plot_form.html).

SUPPLEMENTARY MATERIALS

Supplementary material for this article is available at <http://advances.sciencemag.org/cgi/content/full/1/2/e1500078/DC1>


Fig. S1. Validation of *IGHMBP2* constructs in vitro and in vivo.

Fig. S2. AAV9-*IGHMBP2* administration ameliorates SMARD1 cardiomyopathy.

Movie S1. Gross appearance of an AAV9-*IGHMBP2*-treated *nmd* mouse.

This is an open-access article distributed under the terms of the [Creative Commons Attribution-NonCommercial license](https://creativecommons.org/licenses/by-nc/4.0/), which permits use, distribution, and reproduction in any medium, so long as the resultant use is not for commercial advantage and provided the original work is properly cited.

REFERENCES AND NOTES

1. 
1. K. Grohmann,
2. M. Schuelke,
3. A. Diers,
4. K. Hoffmann,
5. B. Lucke,
6. C. Adams,
7. E. Bertini,
8. H. Leonhardt-Horti,
9. F. Muntoni,
10. R. Ouvrier,
11. A. Pfeufer,
12. R. Rossi,
13. L. Van Maldergem,

14. J. M. Wilmshurst,
15. T. F. Wienker,
16. M. Sendtner,
17. S. Rudnik-Schöneborn,
18. K. Zerres,
19. C. Hübner

, Mutations in the gene encoding immunoglobulin μ -binding protein 2 cause spinal muscular atrophy with respiratory distress type 1. Nat. Genet. **29**, 75–77 (2001).

[CrossRefMedlineWeb of Science](#)

2. [↵](#)
1. M. Eckart,
2. U. P. Guenther,
3. J. Idkowiak,
4. R. Varon,
5. B. Grolle,
6. P. Boffi,
7. L. Van Maldergem,
8. C. Hübner,
9. M. Schuelke,
10. K. von Au

, The natural course of infantile spinal muscular atrophy with respiratory distress type 1 (SMARD1).Pediatrics **129**, e148–e156 (2012).

[Abstract/FREE Full Text](#)

3. [↵](#)
1. F. Porro,
2. P. Rinchetti,
3. F. Magri,
4. G. Riboldi,
5. M. Nizzardo,
6. C. Simone,
7. C. Zanetta,
8. I. Faravelli,

9. S. Corti

, The wide spectrum of clinical phenotypes of spinal muscular atrophy with respiratory distress type 1: A systematic review. *J. Neurol. Sci.* **346**, 35–42 (2014).

[Medline](#)

4. [↵](#)

1. U. P. Guenther,
2. L. Handoko,
3. B. Lagerbauer,
4. S. Jablonka,
5. A. Chari,
6. M. Alzheimer,
7. J. Ohmer,
8. O. Plöttner,
9. N. Gehring,
10. A. Sickmann,
11. K. von Au,
12. M. Schuelke,
13. U. Fischer

, IGHMBP2 is a ribosome-associated helicase inactive in the neuromuscular disorder distal SMA type 1 (DSMA1). *Hum. Mol. Genet.* **18**, 1288–1300 (2009).

[Abstract/FREE Full Text](#)

5. [↵](#)

1. A. Jankowsky,
2. U. P. Guenther,
3. E. Jankowsky

, The RNA helicase database. *Nucleic Acids Res.* **39**, D338–D341(2011).

6. [↵](#)

1. G. A. Cox,
2. C. L. Mahaffey,
3. W. N. Frankel

, Identification of the mouse neuromuscular degeneration gene and mapping of a second site suppressor allele. *Neuron* **21**, 1327–1337 (1998).

[CrossRefMedlineWeb of Science](#)

7. [↵](#)
1. K. D. Foust,
2. E. Nurre,
3. C. L. Montgomery,
4. A. Hernandez,
5. C. M. Chan,
6. B. K. Kaspar

, Intravascular AAV9 preferentially targets neonatal neurons and adult astrocytes. *Nat. Biotechnol.* **27**, 59–65 (2009).

[CrossRefMedlineWeb of Science](#)

8. [↵](#)
1. S. Duque,
2. B. Joussemet,
3. C. Riviere,
4. T. Marais,
5. L. Dubreil,
6. A. M. Douar,
7. J. Fyfe,
8. P. Moullier,
9. M. A. Colle,
10. M. Barkats

, Intravenous administration of self-complementary AAV9 enables transgene delivery to adult motor neurons. *Mol. Ther.* **17**, 1187–1196 (2009).

[CrossRefMedlineWeb of Science](#)

9. [↵](#)
1. A. K. Bevan,
2. S. Duque,
3. K. D. Foust,

4. P. R. Morales,
5. L. Braun,
6. L. Schmelzer,
7. C. M. Chan,
8. M. McCrate,
9. L. G. Chicoine,
10. B. D. Coley,
11. P. N. Porensky,
12. S. J. Kolb,
13. J. R. Mendell,
14. A. H. Burghes,
15. B. K. Kaspar

, Systemic gene delivery in large species for targeting spinal cord, brain, and peripheral tissues for pediatric disorders. *Mol. Ther.* **19**,1971–1980 (2011).

[CrossRefMedline](#)

10. [↵](#)
 1. K. D. Foust,
 2. X. Wang,
 3. V. L. McGovern,
 4. L. Braun,
 5. A. K. Bevan,
 6. A. M. Haidet,
 7. T. T. Le,
 8. P. R. Morales,
 9. M. M. Rich,
 10. A. H. Burghes,
 11. B. K. Kaspar

, Rescue of the spinal muscular atrophy phenotype in a mouse model by early postnatal delivery of *SMN*. *Nat. Biotechnol.* **28**, 271–274 (2010).

[CrossRefMedlineWeb of Science](#)

11. [↵](#)
 1. M. A. Passini,
 2. J. Bu,

3. E. M. Roskelley,
4. A. M. Richards,
5. S. P. Sardi,
6. C. R. O’Riordan,
7. K. W. Klinger,
8. L. S. Shihabuddin,
9. S. H. Cheng

, CNS-targeted gene therapy improves survival and motor function in a mouse model of spinal muscular atrophy. *J. Clin. Invest.* **120**, 1253–1264 (2010).

[CrossRefMedlineWeb of Science](#)

- 12.
1. C. F. Valori,
2. K. Ning,
3. M. Wyles,
4. R. J. Mead,
5. A. J. Grierson,
6. P. J. Shaw,
7. M. Azzouz

, Systemic delivery of scAAV9 expressing SMN prolongs survival in a model of spinal muscular atrophy. *Sci. Transl. Med.* **2**, 35ra42 (2010).

[Abstract/FREE Full Text](#)

13. [↵](#)
1. E. Dominguez,
2. T. Marais,
3. N. Chatauret,
4. S. Benkhalifa-Ziyyat,
5. S. Duque,
6. P. Ravassard,
7. R. Carcenac,
8. S. Astord,
9. A. Pereira de Moura,
10. T. Voit,
11. M. Barkats

, Intravenous scAAV9 delivery of a codon-optimized *SMN1* sequence rescues SMA mice. *Hum. Mol. Genet.* **20**, 681–693 (2011).

[Abstract/FREE Full Text](#)

14. [↵](#)
1. C. Zanetta,
 2. M. Nizzardo,
 3. C. Simone,
 4. E. Monguzzi,
 5. N. Bresolin,
 6. G. P. Comi,
 7. S. Corti

, Molecular therapeutic strategies for spinal muscular atrophies: Current and future clinical trials. *Clin. Ther.* **36**, 128–140 (2014).

[CrossRefMedline](#)

15. [↵](#)
1. S. Corti,
 2. F. Locatelli,
 3. D. Papadimitriou,
 4. C. Donadoni,
 5. R. Del Bo,
 6. M. Crimi,
 7. A. Bordoni,
 8. F. Fortunato,
 9. S. Strazzer,
 10. G. Menozzi,
 11. S. Salani,
 12. N. Bresolin,
 13. G. P. Comi

, Transplanted ALDH^{hi}SSC^{lo} neural stem cells generate motor neurons and delay disease progression of *nmd* mice, an animal model of SMARD1. *Hum. Mol. Genet.* **15**, 167–187 (2006).

[Abstract/FREE Full Text](#)

16.

1. S. Corti,
2. M. Nizzardo,
3. M. Nardini,
4. C. Donadoni,
5. S. Salani,
6. R. Del Bo,
7. D. Papadimitriou,
8. F. Locatelli,
9. N. Mezzina,
10. F. Gianni,
11. N. Bresolin,
12. G. P. Comi

, Motoneuron transplantation rescues the phenotype of SMARD1 (spinal muscular atrophy with respiratory distress type 1). *J. Neurosci.* **29**, 11761–11771 (2009).

[Abstract/FREE Full Text](#)

17. [↵](#)

1. C. Simone,
2. M. Nizzardo,
3. F. Rizzo,
4. M. Ruggieri,
5. G. Riboldi,
6. S. Salani,
7. M. Bucchia,
8. N. Bresolin,
9. G. P. Comi,
10. S. Corti

, iPSC-derived neural stem cells act via kinase inhibition to exert neuroprotective effects in spinal muscular atrophy with respiratory distress type 1. *Stem Cell Reports* **3**, 297–311 (2014).

[Medline](#)

18. [↵](#)

1. K. Grohmann,

2. W. Rossoll,
3. I. Kobsar,
4. B. Holtmann,
5. S. Jablonka,
6. C. Wessig,
7. G. Stoltenburg-Didinger,
8. U. Fischer,
9. C. Hübner,
10. R. Martini,
11. M. Sendtner

, Characterization of *Ighmbp2* in motor neurons and implications for the pathomechanism in a mouse model of human spinal muscular atrophy with respiratory distress type 1 (SMARD1). *Hum. Mol. Genet.* **13**, 2031–2042 (2004).

[Abstract/FREE Full Text](#)

19. [↵](#)
1. T. P. Maddatu,
 2. S. M. Garvey,
 3. D. G. Schroeder,
 4. T. G. Hampton,
 5. G. A. Cox

, Transgenic rescue of neurogenic atrophy in the *nmd* mouse reveals a role for *Ighmbp2* in dilated cardiomyopathy. *Hum. Mol. Genet.* **13**, 1105–1115(2004).

[Abstract/FREE Full Text](#)

20. [↵](#)
1. S. A. Cook,
 2. K. R. Johnson,
 3. R. T. Bronson,
 4. M. T. Davisson

, Neuromuscular degeneration (*nmd*): A mutation on mouse chromosome 19 that causes motor neuron degeneration. *Mamm. Genome* **6**, 187–191 (1995).

[CrossRefMedlineWeb of Science](#)

21. [↵](#)

1. E. Cottenie,
2. A. Kochanski,
3. A. Jordanova,
4. B. Bansagi,
5. M. Zimon,
6. A. Horga,
7. Z. Jaunmuktane,
8. P. Saveri,
9. V. M.Rasic,
10. J. Baets,
11. M. Bartsakoulia,
12. R. Ploski,
13. P. Teterycz,
14. M. Nikolic,
15. R. Quinlivan,
16. M. Laura,
17. M. G. Sweeney,
18. F. Taroni,
19. M. P. Lunn,
20. I. Moroni,
21. M. Gonzalez,
22. M. G. Hanna,
23. C. Bettencourt,
24. E. Chabrol,
25. A. Franke,
26. K. von Au,
27. M. Schilhabel,
28. D.Kabzińska,
29. I. Hausmanowa-Petrusewicz,
30. S. Brandner,
31. S. C. Lim,
32. H. Song,
33. B. O. Choi,
34. R. Horvath,
35. K. W. Chung,
36. S.Zuchner,

37. D. Pareyson,
38. M. Harms,
39. M. M. Reilly,
40. H. Houlden

, Truncating and missense mutations in *IGHMBP2* cause Charcot-Marie Tooth disease type 2. *Am. J. Hum. Genet.* **5**, 590–601 (2014).

22. [↵](#)

1. S. Al-Zaidy,
2. L. Rodino-Klapac,
3. J. R. Mendell

, Gene therapy for muscular dystrophy: Moving the field forward. *Pediatr. Neurol.* **5**, 607–618 (2014).

23. [↵](#)

1. L. G. Chicoine,
2. C. L. Montgomery,
3. W. G. Bremer,
4. K. M. Shontz,
5. D. A. Griffin,
6. K. N. Heller,
7. S. Lewis,
8. V. Malik,
9. W. E. Grose,
10. C. J. Shilling,
11. K. J. Campbell,
12. T. J. Preston,
13. B. D. Coley,
14. P. T. Martin,
15. C. M. Walker,
16. K. R. Clark,
17. Z. Sahenk,
18. J. R. Mendell,
19. L. R. Rodino-Klapac

, Plasmapheresis eliminates the negative impact of AAV antibodies on microdystrophin gene expression following vascular delivery. *Mol. Ther.* **2**, 338–347 (2014).

24. [↵](#)

1. A. D. Ebert,
2. J. Yu,
3. F. F. Rose Jr.,
4. V. B. Mattis,
5. C. L. Lorson,
6. J. A. Thomson,
7. C. N. Svendsen

, Induced pluripotent stem cells from a spinal muscular atrophy patient. *Nature* **457**, 277–280 (2009).

[CrossRef](#)[Medline](#)[Web of Science](#)

25. [↵](#)

1. M. Nizzardo,
2. C. Simone,
3. S. Salani,
4. M. D. Ruepp,
5. F. Rizzo,
6. M. Ruggieri,
7. C. Zanetta,
8. S. Brajkovic,
9. H. M. Moulton,
10. O. Mühlemann,
11. N. Bresolin,
12. G. P. Comi,
13. S. Corti

, Effect of combined systemic and local morpholino treatment on the spinal muscular atrophy $\Delta 7$ mouse model phenotype. *Clin. Ther.* **36**, 340–356.e5 (2014).

[Medline](#)

26. [↵](#)

1. S. Corti,
2. M. Nizzardo,
3. C. Simone,
4. M. Falcone,
5. M. Nardini,
6. D. Ronchi,
7. C. Donadoni,
8. S. Salani,
9. G. Riboldi,
10. F. Magri,
11. G. Menozzi,
12. C. Bonaglia,
13. F. Rizzo,
14. N. Bresolin,
15. G. P. Comi

, Genetic correction of human induced pluripotent stem cells from patients with spinal muscular atrophy. *Sci. Transl. Med.* 4, 165ra162 (2012).

27. **Acknowledgments:** We wish to thank the Associazione Amici del Centro Dino Ferrari for their support. **Funding:** This work was funded by Italian Ministry of Health grant GR-2010-2309229 to M.N. **Author contributions:** M.N. and C.S. performed in vivo experiments; S.D. performed in vitro experiments; R.D.B. performed molecular biology experiments; S.S. performed proteomic analysis; F.R. and P.R. performed neuropathological analysis; K.F. worked on AAV vectors design and production; M.N. participated in all the experiments; N.B., G.P.C., and B.K. contributed ideas and supported the work; S.C. and M.N. conceived the experiments and wrote the manuscript; C.S. and K.F. contributed in the manuscript writing. **Competing interests:** B.K. is on the board of directors of Avexis, a clinic-stage gene therapy platform company.

- Received for publication 20 January 2015.
- Accepted for publication 15 February 2015.
- Copyright © 2015, The Authors